Unique Superparamagnetic-like Behavior Observed in Non-π-delocalized Nitroxide Diradical Compounds Showing Discotic Liquid Crystalline Phase

Yusa Takemoto, Elena Zaytseva, Katsuaki Suzuki, Naoki Yoshioka, Yoichi Takanishi, Masahiro Funahashi, Yoshiaki Uchida, Takuya Akita, Jayeong Park, Shuichi Sato, et al.

Unique Superparamagnetic-like Behavior Observed in Non-π-delocalized Nitroxide Diradical Compounds Showing Discotic and Smectic Liquid Crystalline Phases

Yusa Takemoto,[1] Elena Zaytseva,[1,2] Katsuaki Suzuki,[1] Naoki Yoshioka,[3] Yoichi Takanishi,[4] Masahiro Funahashi,[5] Yoshiaki Uchida,[6] Takuya Akita,[6] Jayeong Park,[1] Shuichi Sato,[1] Simon Clevers,[7] Gérard Coquerel,[7] Dmitrii G. Mazhukin,[2,8] Satoshi Shimono,[1] Masahito Sugiyama,[1] Hiroki Takahashi,[1] Jun Yamauchi,[1] Rui Tamura*[1]

[1]Graduate School of Human and Environmental Studies, Kyoto University, Kyoto 606-8501, Japan

[2]N. N. Vorozhtsov Novosibirsk Institute of Organic Chemistry, Siberian Branch of Russian Academy of Sciences, 9 Akademika Lavrentieva Ave., Novosibirsk 630090, Russia

[3]Department of Applied Chemistry, Keio University, Yokohama, Kanagawa 223-8522, Japan

[4]Graduate School of Science, Kyoto University, Kyoto 606-8502, Japan

[5]Department of Advanced Materials Science, Faculty of Engineering, Kagawa University, Takamatsu, Kagawa 761-0396, Japan

[6]Graduate School of Engineering Science, Osaka University, Toyonaka, Osaka 560-8531, Japan

[7]Normandie Université, SMS, EA 3233, Univ Rouen, Crystal Genesis Unit, 76821 Mont Saint-Aignan Cedex, France

[8]Novosibirsk State University, 2 Pirogova St., Novosibirsk 630090, Russia

Abstract

The development of metal-free magnetic nanocrystalline or soft materials whose motion can be controlled by a weak magnetic field at ambient temperature is one of challenging subjects in magnetic materials chemistry. We report that a unique superparamagnetic-like behavior and a large 'positive magneto-LC effect' were observed in the solid phases and the liquid crystalline (LC) phases, respectively, of novel achiral non-π-delocalized nitroxide diradical compounds **1** which showed a rare phase transition behavior; the existence of polymorphism in the solid phases (solids I and II) at low temperatures and the coexistence of hexagonal columnar and smectic LC phases at high temperatures. The gradual formation of chiral helical columnar structure in the hexagonal columnar phase was confirmed by a preliminary SHG measurement. By SQUID magnetization measurement, it was revealed that (1) **1** possessed an unusual temperature-independent magnetic susceptibility ($\chi_{TIM} > 0$) component in the original nanocrystalline solid I which was responsible for the observed superparamagnetic-like behavior at low magnetic fields and did not arise from the contamination by extrinsic magnetic metal or metal ion impurities, besides ordinary temperature-dependent paramagnetic susceptibility ($\chi_{para} > 0$) and temperature-independent diamagnetic susceptibility

(χ_{dia} < 0) components, (2) a large increase in molar magnetic susceptibility (χ_M) (positive magneto-LC effect) occurred at the solid I-to-liquid crystal transition in the heating run, and (3) the χ_M increase was preserved as an additional χ_{TIM} increase in the resulting polymorphic nanocrystalline solid II by cooling. The origin of this unique magnetic behavior can be rationalized in terms of the formation of magnetically inhomogeneous domains with intermolecular short contacts in the nanocrystalline solid phases and their enlargement in the LC phases under low magnetic fields. Such superparamagnetic-like properties would be applicable to the development of various metal-free magnetic advanced materials.

INTRODUCTION

Liquid crystalline (LC) phases which can exhibit non-linear responses to external stimuli, such as temperature, pressure, and electric or magnetic field, or additives like chiral dopants, due to the coherent collective molecular motion, are regarded as a sort of dynamic nonequilibrium 'complexity' system.[1-3] Therefore, magnetic LC materials have attracted a great attention as soft materials because magnetic fields can influence the optical and electric properties of liquid crystals.[4-8] For example, they are anticipated to exhibit unique magnetic interactions leading to unconventional magnetoelectric[9-12] or magneto-optical properties[13-15] in the LC state. However, there had been no prominent study on this interesting topic, because the majority of magnetic liquid crystals were highly viscous transition or lanthanide metal-containing metallomesogens which were not always suitable to these studies.[4-8] Since 2008 it has been revealed that a sort of spin glass (SG)-like inhomogeneous magnetic interactions (average spin-spin interaction constant $\bar{J}$ > 0) occur in the various chiral or achiral, rod-like LC phases of monoradical and biradical compounds with one or two stable chiral five-membered nitroxide units in the central core position and thereby with a negative dielectric anisotropy ($\Delta\varepsilon$ < 0) under low magnetic fields (< 0.1 T).[16,17] This unique magnetic phenomenon, an increase in the molar magnetic susceptibility (χ_M) at the crystal-to-liquid crystal phase transition, was referred to as 'positive magneto-LC effect'.[18,19] Although the detailed mechanism is still under investigation, this large χ_M increase was proved to be not due to the molecular reorientation effect caused by the molecular magnetic anisotropy ($\Delta\chi$)[16,20]. Moreover, the first observation of 'magnetoelectric effect (or coupling)' at as high as 75 °C was achieved for the LC monoradical compound showing both the ferroelectricity and the positive magneto-LC effect in a surface-stabilized liquid crystal cell.[21-23]

Meanwhile, it was anticipated that i) the positive magneto-LC effect could be induced under low magnetic fields in the columnar LC phases of organic radical compounds as well, by a judicious molecular design so as to avoid the strong π-π dimer formation which results in the antiferromagnetic interactions (or negative magneto-LC effect), and thereby ii) a magnetic field-controlled photoinduced hole transport in the semiconducting columnar phase may be feasible due to the relatively high-lying singly occupied molecular orbital (SOMO) and its delocalization on the aromatic core in comparison to their closed-shell analogue. In 2014 an achiral π-delocalized hexa-peri-hexabenzocoronene derivative carrying a conjugated *tert*-butyl nitroxide moiety was reported to show the positive magneto-LC effect in the hexagonal columnar LC

phase,[24] whereas disc-like triphenylenes carrying a non-conjugated cyclic nitroxide monoradical group[25] and other three types of disc-like compounds with π-delocalized photoluminescent tris(2,4,6-trichlorophenyl)methyl,[26] and semiconducting 6-oxoverdazyl[27,28] or benzo[e][1,2,4]triazinyl monoradical moieties[29] as the spin source did not exhibit the positive magneto-LC effect in their achiral columnar LC state.

Here we report the observation of a unique superparamagnetic-like behavior and a large positive magneto-LC effect in the nanocrystalline solid phases and the hexagonal columnar (Col_h) and smectic (Sm) LC phases, respectively, of non-π-delocalized nitroxide diradical compounds **1** and discuss the origin of this magnetic phenomenon in terms of the formation and enlargement of magnetically inhomogeneous domains in the solids and LC phases.

RESULTS AND DISCUSSION

Preparation and EPR spectra of (*R*,*S*)-1. The meso nitroxide diradical (*R*,*S*)-**1** was prepared by the condensation of the dicarboxylic acid (*R*,*S*)-**2**, which was derived from the bisnitrone **4**,[30] and two equiv of 2-[3,4,5-tris(hexadecyloxy)phenyl]ethanamine (**5**) using 4-(4,6-dimethoxy-1,3,5-triazin-2-yl)-4-methylmorpholinium chloride (DMT-MM)[31] and a catalytic amount of *N*-methylmorpholine (NMM) in dichloromethane (Scheme 1 and Section 2 in Supporting Information for the details).

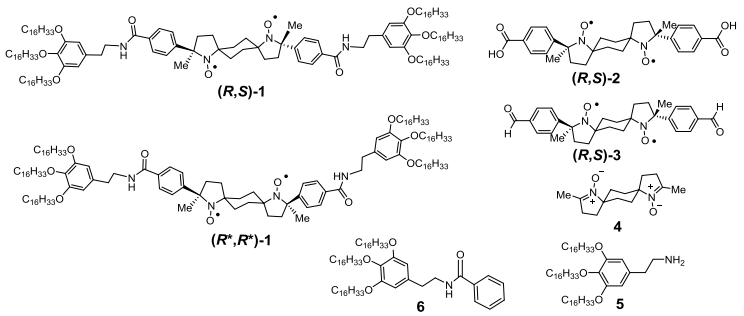

Scheme 1. Molecular structures of compounds **1**-**6**.

The EPR spectra of (*R*,*S*)-**1** to (*R*,*S*)-**3** were measured in the diluted (1.0×10^{-4} M) THF solutions at 298 and 123 K (Fig. 1). At 298 K, all spectra of these three samples showed five peaks (Fig. 1a–d), suggesting strong intramolecular spin-spin exchange interactions in solution. The broadening of second and fourth lines in the spectra of (*R*,*S*)-**1** and (*R*,*S*)-**2** was attributed to the modulation of the exchange interactions induced by internal motion of the cyclohexane ring due most likely to the presence of strong intermolecular interactions formed by hydrogen bonds (Fig. 1a,b). A similar spectral broadening, referred to as the 'alternating linewidth effect', was reported for analogous 1,4-bis(4',4'-dimethyloxazolidine-3'-oxyl)cyclohexane by Rassat group in 1975.[32] Our EPR experimental data shown in Fig. 1 were consistent with those.

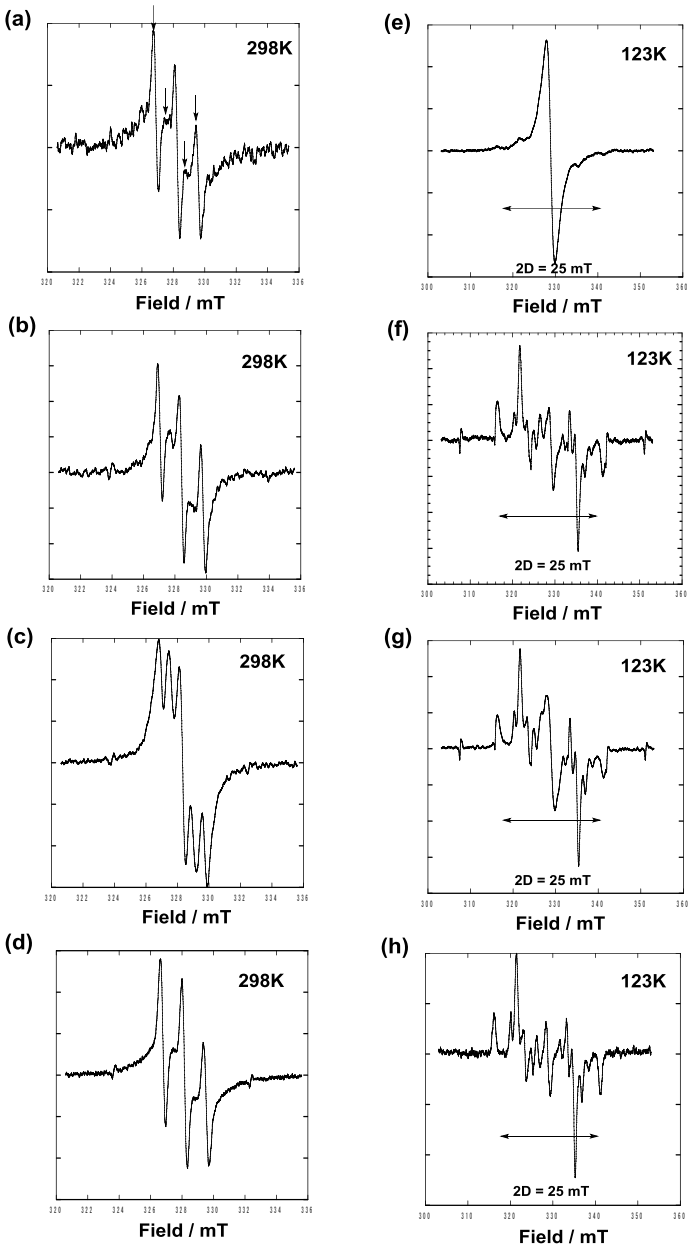

Figure 1. ESR spectra in THF of (a) (*R*,*S*)-**1** (1×10^{-4} M), (b) (*R*,*S*)-**2** (1×10^{-4} M), (c) (*R*,*S*)-**3** (1×10^{-4} M) and (d) a mixture of (*R*,*S*)-**1** (1×10^{-4} M) and **5** (1×10^{-2} M) at 298K, and (e) (*R*,*S*)-**1** (1×10^{-4} M), (f) (*R*,*S*)-**2** (1×10^{-4} M), (g) (*R*,*S*)-**3** (1×10^{-4} M) and (h) a mixture of (*R*,*S*)-**1** (1×10^{-4} M) and **5** (1×10^{-2} M) at 123 K. The internal standard Mn^{2+} was used to measure the spectra in panels (a)–(d), (f) and (g).

At 123 K the spectrum of (*R*,*S*)-**1** diluted by 100-fold with **6** (Fig. 1h), characteristic of a triplet spin state without axial symmetry, was similar to the spectra of (*R*,*S*)-**2** and (*R*,*S*)-**3** (Fig. 1f, g), although free (*R*,*S*)-**1** showed a broad singlet spectrum due to the substantial molecular aggregation even at such a low concentration (Fig. 1e). The intramolecular distance between two nitroxide radical groups for these three samples was estimated to be 6.06 Å by point dipole approximation, which was in good agreement

with that obtained from the crystal structure of (*R*,*S*)-**2** (Fig. S1). The energy difference between the singlet and triplet states in the molecule of (*R*,*S*)-**2** was calculated by density functional theory (DFT) calculations at the UB3LYP/6-31G* level (Gaussian03) based on the same crystal structure (Sections 3 and 4 in SI); the singlet state was more stable by 22.0 K than the triplet state.

Characterization of the LC phase of (*R*,*S*)-1. The phase transition behavior of (*R*,*S*)-**1** was characterized by differential scanning calorimetry (DSC), polarized optical microscopy (POM), and X-ray diffraction (XRD) and small angle X-ray scattering (SAXS) analyses (Fig. 2).

At least four phases were characterized for (*R*,*S*)-**1**. Among them, the hexagonal columnar (Col_h) and smectic (Sm) phases were enantiotropically related; DSC analysis indicated that the phase transition of original solid I occurred at 83.3 °C to give a Col_h phase, followed by the transition at 99.9 °C to an Sm phase with pseudo-isotropic texture in the first and second heating runs (Fig. 2a). These two LC phases showed a small angle diffraction peak at a different angle of 2θ = 2.14° or 2.41°, together with a similar diffuse band at around 2θ = 20° (Fig. 2d, e). However, by POM observation in the first cooling run at a scanning rate of 5 or 10 °C min^{-1}, only a fan-like or focal conic texture corresponding to the Col_h phase was observed under random conditions or homogeneous planar boundary conditions in a thin sandwich cell (4 μm thickness), respectively (Fig. 2b,c). Furthermore, the DSC thermograms in the first and second heating runs were very different regarding the solid-to-LC transition temperature (83.3 and 36.3 °C, respectively) due to the existence of two polymorphs (solids I and II) (Fig. 2a), which was confirmed by XRD analysis (Fig. 2h,i). Furthermore, from the broad XRD peaks and large enthalpies of transition ΔH's (132.8 and 63.3 kJ mol^{-1}) at around 83 and 36 °C for solids I and II in the first and second heating runs, respectively, it was concluded that both solids are nanocrystalline.

To characterize the LC phases of (*R*,*S*)-**1** accurately, the LC phase transition behavior was investigated in detail by two-dimensional SAXS measurement. Since the SAXS pattern observed at 80 °C at a cooling rate of 10 °C min^{-1} from the isotropic phase (130 °C) represented hexagonal symmetry on the (10) plane (Fig. 2f), the LC phase was determined to be the Col_h with a lattice constant of a = 51.8 Å, although the (1,1) reflection was not observed (Fig. 2d and Fig. 3a,b).[33] The diffuse band at around 4.4 Å (2θ = 20°) is typically attributed to the disordered packing of aliphatic chains and rigid cores characteristic of the LC phase (Fig. 3a,b). The number (Z) of molecules in the unit cell of the Col_h phase of (*R*,*S*)-**1** could be estimated to be three from the experimental data, by assuming the density (ρ) value of (*R*,*S*)-**1** to be 1.04 g cm^{-3} and the lattice constant c to be 4.4 Å (Fig. 3a,b; Section 5 and Fig. S2 in SI).[34,35] This result suggests the existence of a trimer in the unit cell (Fig. 3c). Interestingly, the SAXS pattern at 80 °C observed at a cooling rate of as slow as 0.5 °C min^{-1} from the isotropic phase (130 °C) represented the coexistence of the Col_h (d = 44.8 Å) and Sm (d = 38.4 Å) phases, which continued during the cooling process until the transition to solid II (Fig. 2g). Thus, in case of (*R*,*S*)-**1**, only the Col_h phase grew by fast cooling from the isotropic phase (Fig. 2f), while by very slow cooling from the isotropic phase, the Sm phase appeared first,

followed by the appearance of the hexagonal phase to result in the coexistence of the two phases (Fig. 2g), which was also confirmed by POM observation in the second heating run (Fig. S3). This is a very rare case of the coexistence of two LC phases over a wide temperature range.[36,37]

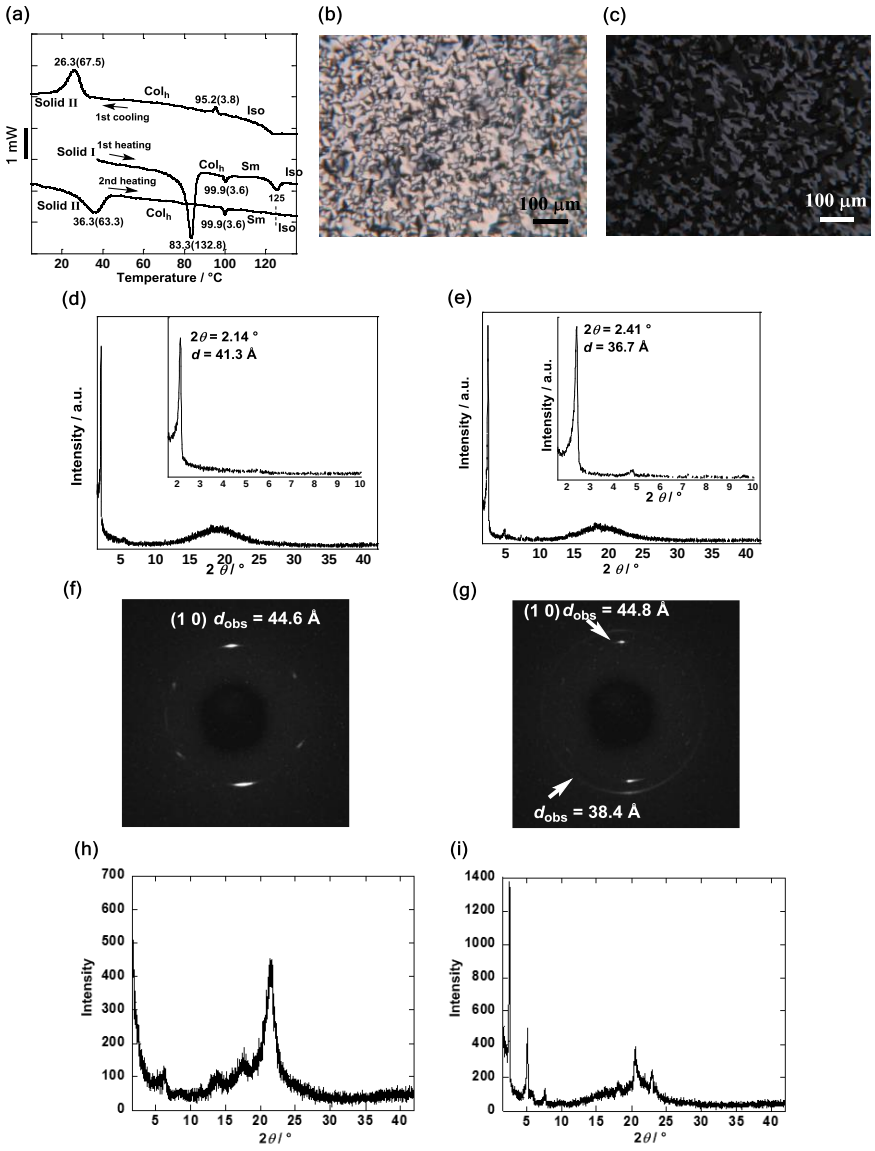

Figure 2. Characterization of the LC phase of (*R*,*S*)-**1**. (a) DSC curves at a scanning rate of 10 °C min^{-1} in the first heating and cooling runs, and the second heating run. Phase transition temperatures (°C) and enthalpies (in parentheses, kJ mol^{-1}) are indicated. Polarized optical microphotographs of the Col$_h$ phase at 80 °C in the first cooling run: (b) the fan-like texture under random conditions and (c) the focal conic texture under homogeneous planar boundary conditions in a 4 μm sandwich cell. XRD patterns of (d) the Col$_h$ phase at 90 °C and (e) the Sm phase at 100 °C in the first heating run, and each inset indicates the magnification below $2\theta = 10°$. Two-dimensional SAXS patterns at 80 °C in the cooling run: (f) the Col$_h$ phase observed at a cooling rate of 10 °C min^{-1} from the isotropic phase (130 °C) and (g) the coexistence

of the Col_h and Sm phases observed at a cooling rate of as slow as 0.5 °C min^{-1} from the isotropic phase (130 °C). XRD patterns in the solid phases at 30 °C: (h) Solid I before the first heating and (i) solid II before the second heating.

(a)

Compound	2 θ (°)	d_{obs} (Å)[a]	hk[b]	Mesophase Lattice parameters[c]
(*R*,*S*)-**1**	1.98[d]	44.6	10	a = 51.8 Å c = 4.4 Å Col_h S = 3102.0 Å^2 V = 13772.9 Å^3 ρ = 1.04 g cm^{-3} Z = 3
	20[e]	4.4	halo[f]	

[a] d_{obs} is the observed diffraction spacing. [b] hkl is the indexation of the two-dimensional lattice. [c] S is the lattice area; $S = a^2*2/\sqrt{3}$ for the Col_h, $a = d_{10}*2/\sqrt{3}$ for Col_h phase, V is molecular volume; $V = a{\cdot}a2/\sqrt{3}{\cdot}c$, ρ is the volume mass density, and Z is the number of molecules in each disc layer. [d] SAXS data. [e] XRD data. [f] Broad reflection of disordered packing of aliphatic chains and rigid cores characteristic of an LC phase.

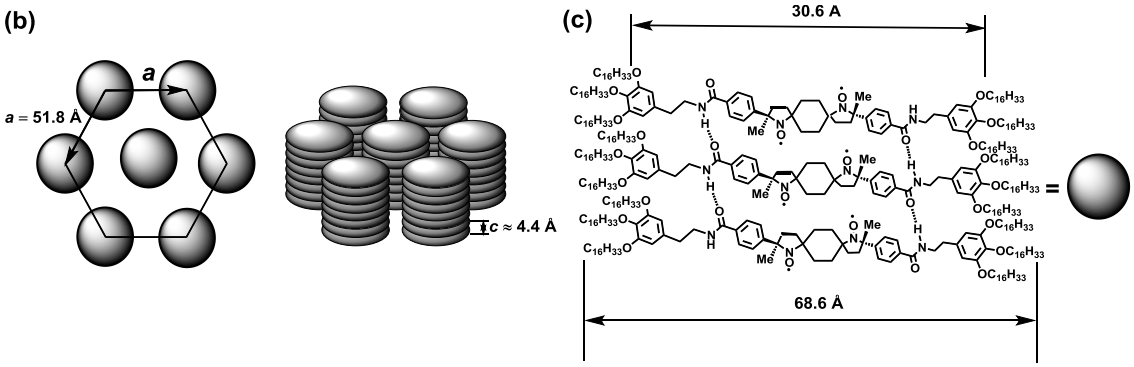

Figure 3. (a) The proposed indexing, lattice parameters, and observed spacing corresponding to SAXS data measured at 80 °C in the cooling run of (*R*,*S*)-**1** (Fig. 2f) and XRD data (Fig. 2d). Hexagonal columnar structure and molecular arrangement in the Col_h phase of (*R*,*S*)-**1**, (b) hexagonal lattice with the constant a derived from d_{obs} = 44.6 Å and the columnar structure and (c) one of possible trimer structures formed by hydrogen bonds in one layer. The approximate molecular length (68.6 Å) and core length (30.6 Å) of (*R*,*S*)-**1** were obtained by MM2 calculations.

To discuss the possibility of the trimer structure of (*R*,*S*)-**1** (Fig. 3c), the variable-temperature micro-ATR-FTIR spectroscopic analysis was performed in the heating and cooling runs between 30 and 100 °C (Fig. S4). This analysis indicated that (1) no appreciable change in the spectral peak position, intensity and shape was noted over the entire temperature range and that (2) the broad NH stretching vibration at around 3330 cm^{-1} and the C=O stretching vibration at 1640 cm^{-1} which are ascribed to the formation of hydrogen bond were observed uniformly in the condensed phases. Accordingly, the trimer structure is most likely formed by intermolecular hydrogen bonds between amide CO and NH groups of

(*R*,*S*)-**1** (Fig. 3c), and this structure is assumed to be retained during all phase transitions between solids and LC phases in both heating and cooling runs.[38]

Furthermore, to learn whether a helical columnar structure is formed in the LC and solid phases, the temperature-resolved second harmonic generation (TR-SHG) microscopy was preliminarily performed for (*R*,*S*)-**1** with an excitation wavelength of 1200 nm and SHG emission at 600 nm in the presence of a magnetic field (< 0.5 T). For solid I at 26.5 °C, only a weak SHG was detected. Because the intensity of third harmonic generation (THG) emission was about seven times higher than that of the SHG one (Section 12 and Fig. S8 in SI), it was concluded that the detected SHG emanated only from the surface of crystals, indicating that the solid I was centrosymmetric. In contrast, when the solid I was heated at a rate of 10 °C min^{-1} and the resulting LC phase was annealed at 90 °C, the distinct SHG images were recorded at 0, 5 and 10 min after the beginning of annealing. The observed SHG intensity was increased with the elapse of time, suggesting that the chiral Col_h phase gradually grew (Fig. S9 in SI).

Unique magnetic properties of LC compounds 1. The temperature dependence of molar magnetic susceptibility (χ_M) was measured for compounds **1** at a magnetic field of 0.05 T on a SQUID magnetometer using a paramagnetic aluminum foil to minimize the experimental error at high temperatures. Consequently we found that LC compound **1**(95:5) composed of a 95:5 mixture of (*R*,*S*)-**1** and racemic diastereomers (*R**,*R**)-**1** showed a quite unique magnetic behavior in the first heating and cooling runs (Fig. 4 and 5), whereas pure (*R*,*S*)-**1** displayed a fairly different magnetic aspect from that of **1**(95:5) (Fig. 6 and 7).

First, the experimental results on the magnetic properties of **1**(95:5) are described. Here χ_M is defined as the sum of temperature-dependent paramagnetic susceptibility ($\chi_{para} > 0$), temperature-independent magnetic one ($\chi_{TIM} > 0$) unique to **1**(95:5), and temperature-independent diamagnetic one ($\chi_{dia} < 0$) (eq 1), due to the reason mentioned below.

$$\chi_M = \chi_{para} + \chi_{TIM} + \chi_{dia} \quad (1)$$

The χ_{dia} value of -1.6×10^{-3} emu mol^{-1} calculated according to the Pascal's constants was used for this study, because only the sum of χ_{TIM} and χ_{dia} values for the solids can be experimentally obtained as the temperature-independent component by χ_M-T^{-1} plots between100 and 250 K according to the Curie-Weiss law.

The antiferromagnetic interactions showing a χ_{para} (and χ_M) maximum at 23 K were observed most likely due to the intramolecular magnetic interactions with a singlet ground state which was presumed by the DFT calculations of (*R*,*S*)-**2** (Section 4 in SI). In fact, the experimental χ_{para} vs T curve was well fitted to the Bleany-Bowers equation (antiferromagnetic dimer model) (eq 2)[39] with $2J/k_B = -39.6$ K in the temperature range from 16 to 100 K when the sum of χ_{TIM} and χ_{dia} values were subtracted from the χ_M value (Fig. 4a). However, the experimental data above 100 K deviated from this fitting curve, indicating

that $2J/k_B$ is temperature-dependent most likely because of the molecular structural change resulting from the thermal motion of the cyclohexane ring in the solid I.

$$\chi_{para} = \frac{2N_A g^2 \beta^2}{3k_B T}\left[1+\frac{1}{3}\exp\left(-\frac{2J}{k_B T}\right)\right]^{-1} \quad (2)$$

Therefore, the Curie-Weiss fitting was implemented for the solids in the first heating and cooling runs, and the second heating run between 100 and 250 K (eq 3 and Fig. 4h).

$$\chi_{para} = C/(T-\theta) \quad (3)$$

According to eqs 1 and 3, $\chi_{TIM} + \chi_{dia} = +1.24 \times 10^{-3}$ emu mol^{-1}, Weiss constant $\theta = 0$ K, and Curie constant $C = 0.64$ emu K mol^{-1} were obtained in the first heating run (Fig. 4a, b). The average θ value of nearly zero between 100 and 250 K suggests that the θ is temperature-dependent most likely due to the interplay between intramolecular antiferromagnetic interactions ($\theta < 0$) and intermolecular ferromagnetic interactions ($\theta > 0$). It is noteworthy that the solid I contains a χ_{TIM} component of as large as $+2.8 \times 10^{-3}$ emu mol^{-1} in this temperature range, in addition to an ordinary Curie-Weiss paramagnetic component, e.g., the $\chi_{para} = +2.5 \times 10^{-3}$ emu mol^{-1} at 250 K. Such an existence of a χ_{TIM} component in the original solid phase was not observed in small rod-like nitroxide radical compounds which exhibited a positive magneto-LC effect.[16,18]

Another important result is a large χ_M increase at the solid I-to-Col$_h$ phase transition (83 °C) in the first heating run (Fig. 4c,d), which was associated with the formation of chiral helical columnar structure in the Col$_h$ phase. This χ_M increase was preserved during the first cooling and second heating runs and such a magnetic behavior was observed for various rod-like LC nitroxide radical compounds, too (Fig. 4e).[16-18] The χ_{TIM} values obtained by subtracting the calculated χ_{dia} value (-1.6×10^{-3} emu mol^{-1}) from the experimental ($\chi_{TIM} + \chi_{dia}$) value ($+1.24 \times 10^{-3}$, $+2.14 \times 10^{-3}$ and $+1.90 \times 10^{-3}$ emu mol^{-1}) between 100 and 250 K in the first heating and cooling runs and the second heating run were $+2.8 \times 10^{-3}$, $+3.7 \times 10^{-3}$ and $+3.5 \times 10^{-3}$ emu mol^{-1}, respectively (Fig. 4h). This χ_M or χ_{TIM} increase ($+0.90 \times 10^{-3}$ emu mol^{-1}) between the first heating and cooling runs was much larger than that arising from the molecular reorientation effect caused by the small molecular $\Delta\chi$,[20] as shown afterward (Fig. 6a. 9a and 10a). The increase in the χ_{TIM} value between solids I and II was confirmed by measuring the magnetic-field (H) dependence of molar magnetization (M) at 150 and 353 K by the first and second heating (Fig. 5). The M highly deviated from the linearity below 1000 Oe, implying the existence of a χ_{TIM} component responsible for the observed superparamagnetic-like M-H behavior in the solids I and II. Furthermore, the deviation of M in the Col$_h$ phase at 353 K was larger than that in the solid I at 150 K in the first heating (Fig. 5b, f) and comparable to that in the solid II at 150 K in the second heating (Fig. 5d, f). Thus, the observed saturated M (2 ~ 4 emu mol^{-1}) with respect to the deviated M component (Fig. 5b, d, f) turned out to correspond to the respective χ_{TIM} values. Such a superparamagnetic-like M-H behavior was observed in the Sm and isotropic phases, too, although the plots fairly scattered at higher temperatures.

The existence of χ_{TIM} in the original solid I was not due to the aluminum foil used, since the Al

blank values were carefully subtracted from the experimental raw data and the χ_M of Al was actually as low as +1.5~1.8 x 10^{-5} emu mol^{-1}, if any. Furthermore, almost negligible contamination by extrinsic magnetic metal or metal ion impurities in **1**(95:5) was verified by inductively coupled plasma-atomic emission spectroscopy (ICP-AES), too (Section 8 in SI and Table S1); e.g., the iron content was 1.3 μg/g (or ppm) which corresponded to 0.62 emu mol^{-1} and was far less than the observed saturated *M* of 2 to 4 emu mol^{-1} (Fig. 5), the nickel content was only 0.6 μg/g, and the manganese content was less than the detection limit of 0.2 μg/g. Further proofs of the negligible contamination by extrinsic magnetic metal or metal ion impurities in compounds **1** by SQUID measurement are given in the following sections including Figs. 6-9.

Thus, the large χ_M increase observed in the LC (Col_h and Sm) phases in the first heating run corresponded to the 32% χ_{TIM} increase in the solid II in the first cooling run, compared with the solid I. It is noteworthy that the χ_M increase at the solid I-to-Col_h transition occurred only in the presence of a magnetic field. Namely, either of the χ_M or χ_{TIM} increase was not seen in the first heating (up to 390 K) or cooling run, respectively, in the absence of a magnetic field above 300 K. In this case, the χ_M increase appeared in the second heating run up to 390 K at a magnetic field of 0.05 T and was preserved as the χ_{TIM} increase, giving a χ_M-*T* scheme almost similar to that in Fig. 4c. In summary, these results indicate that (1) the original solid I already contained a χ_{TIM} component, which increased in the solid II by heating to the LC phase followed by cooling under low magnetic fields and (2) the χ_M increase at the solid I-to-Col_h phase transition does not arise from the release of antiferromagnetic interactions observed in the solid I below 100 K nor the small molecular $\Delta\chi$. It is reasonable to consider that this unique magnetic transition behavior should be ascribed to an enlargement of magnetically inhomogeneous domains in the LC phase, which leads to the observed χ_M and χ_{TIM} increases in the LC and solid II phases, respectively. Such a unique magnetic phenomenon is reminiscent of the magnetic properties of spin glass materials through thermal processing.[40,41]

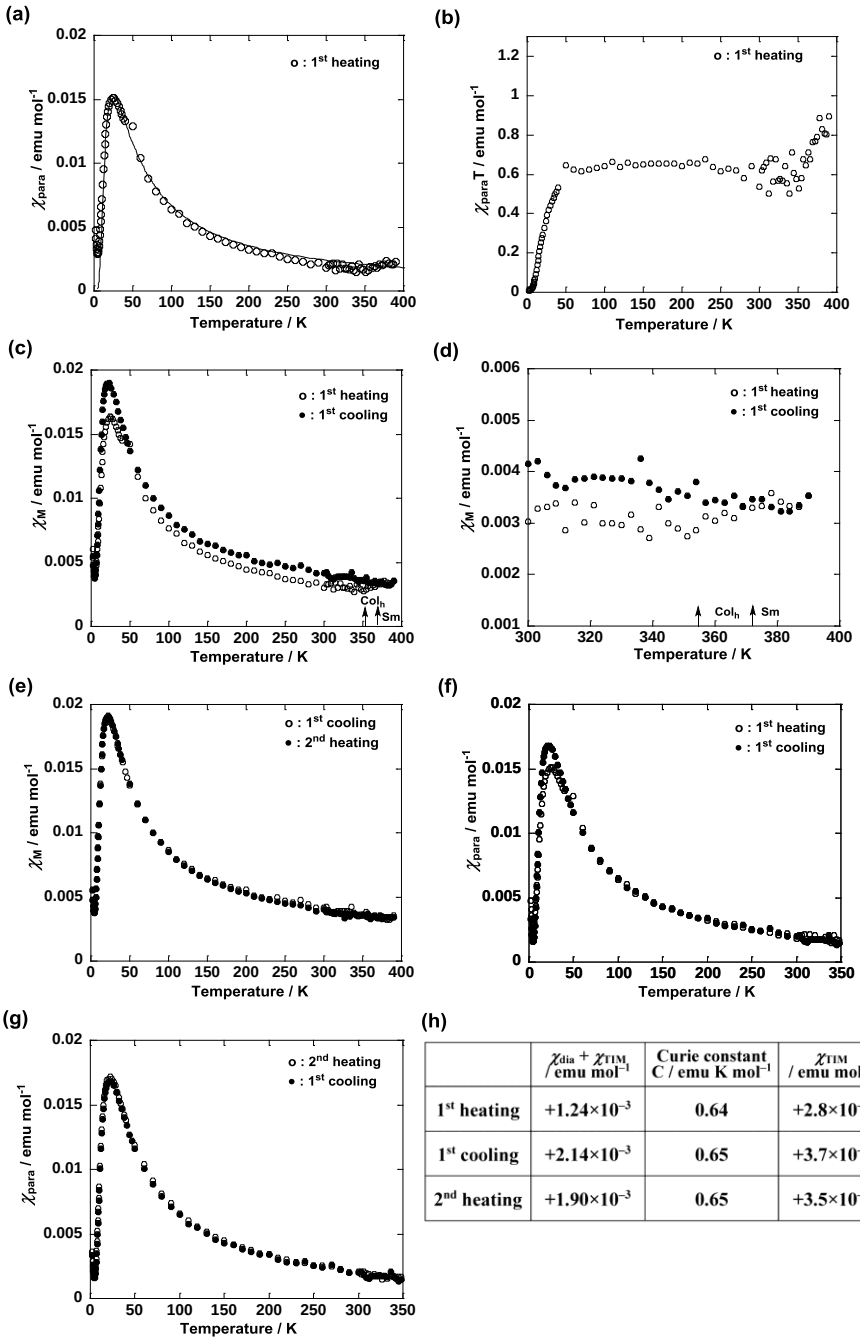

(h)

	$\chi_{dia} + \chi_{TIM}$ / emu mol^{-1}	Curie constant C / emu K mol^{-1}	χ_{TIM} / emu mol^{-1}
1st heating	+1.24×10^{-3}	0.64	+2.8×10^{-3}
1st cooling	+2.14×10^{-3}	0.65	+3.7×10^{-3}
2nd heating	+1.90×10^{-3}	0.65	+3.5×10^{-3}

Figure 4. Temperature dependence of (a) χ_{para} in the first heating run (the solid line calculated by using the Bleany-Bowers equation with $2J/k_B = -39.6$ K), (b) $\chi_{para}T$ in the first heating, (c) χ_M in the first heating and cooling runs, (d) χ_M by magnification (between 300 and 400 K) of panel c, (e) χ_M in the first cooling and second heating runs, (f) χ_{para} in the first heating and cooling runs, and (g) χ_{para} in the first cooling and second heating runs, measured for **1**(95:5) at 0.05 T in the temperature range between 2 and 390 K using a paramagnetic aluminum foil. (h) Obtained magnetic constants and χ_{TIM} values in the first heating and cooling runs, and the second heating run.

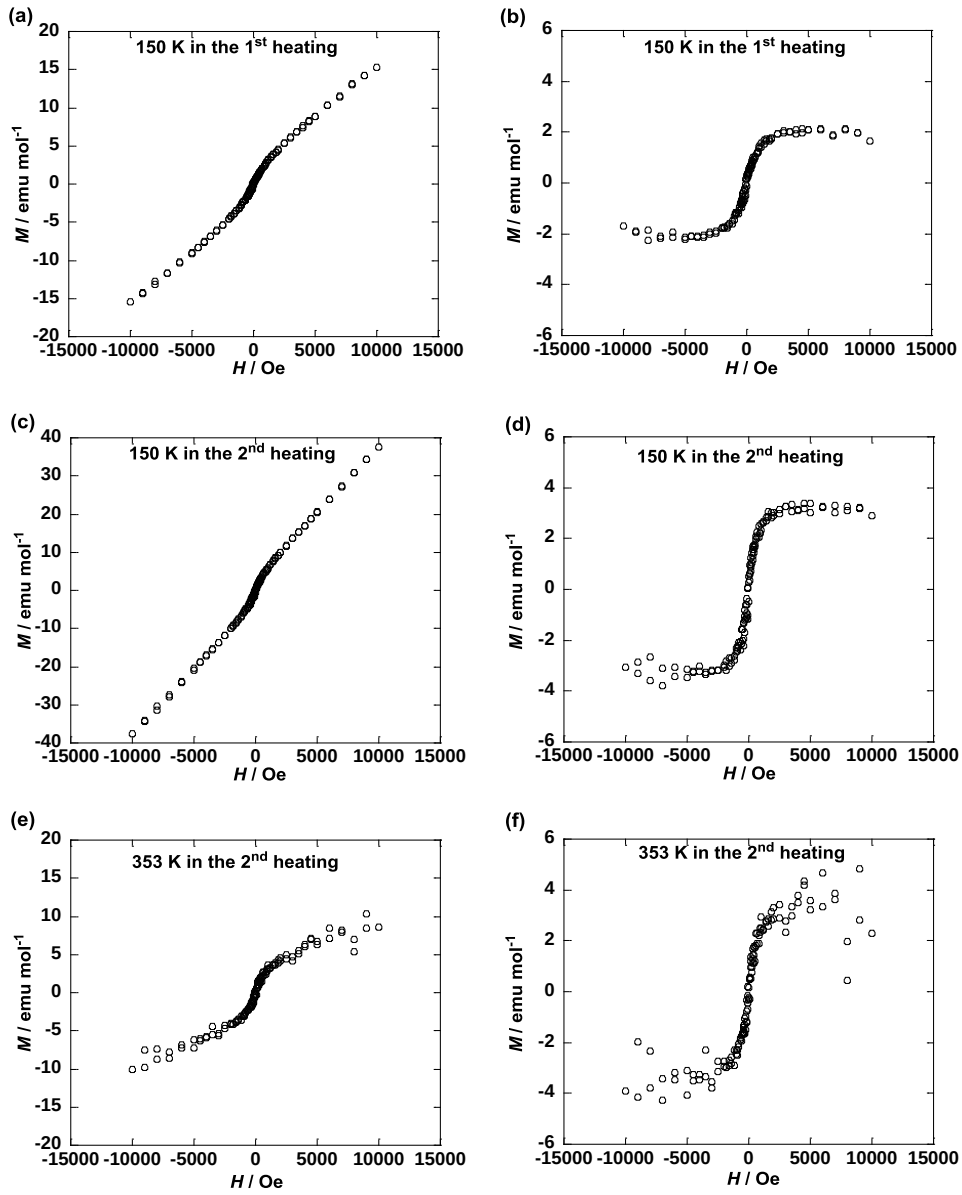

Figure 5. Magnetic field (*H*) dependence of molar magnetization (*M*) for **1**(95:5) (a) in the solid I at 150 K by the first heating from 2 K, (b) after correction of the oblique linear base line to the horizontal one in panel a, (c) in the solid II at 150 K by the second heating after the first heating up to 390 K followed by cooling to 2 K at 0.05 T, (d) after correction of the oblique linear base line to the horizontal one in panel c, (e) in the Col_h phase at 353 K by the second heating, and (f) after correction of the oblique linear base line to the horizontal one in panel e.

To investigate the influence of the minor component (*R**,*R**)-**1** on the magnetic properties of the major component (*R*,*S*)-**1** in **1**(95:5), (*R**,*R**)-**1** was synthesized from (*R**,*R**)-**3** (Section 2 in SI). (*R**,*R**)-

1 with a melting point of 54.3 °C (DSC analysis) did not show an LC phase and thereby either the superparamagnetic-like *M-H* behavior or the χ_M increase in the first heating and cooling, and second heating runs at 0.05 T (Fig. 8). Noticeably, in contrast, although pure (*R*,*S*)-**1** showed neither the superparamagnetic-like *M-H* behavior nor the χ_M increase in the first heating run at 0.05 T (Fig. 6a,b and 7a,b), a superparamagnetic-like *M-H* behavior and a χ_M increase were revived by the first cooling from the isotropic phase and in the second heating run, respectively, at 0.05 T (Fig. 6 and 7c-f). These results proved almost negligible contamination of extrinsic magnetic metal or metal ion impurities in (*R*,*S*)-**1** and (*R**,*R**)-**1** and provided the first observation of an increase in magnetic interactions only by thermal processing for (*R*,*S*)-**1**. Such a thermal phenomenon was often observed in the metallic spin glass materials[40,41] and spin glass-like poly(phenylacetylene) π-radicals.[42]

Furthermore, it was confirmed that so long as compounds **1** composed of the major (*R*,*S*)-**1** and minor (*R**,*R**)-**1** components were used, (1) the occurrence of the superparamagnetic-like *M-H* behavior in the solids I and II and (2) the large χ_M increase at the solid I-to-Col_h phase transition in the first heating run were fully reproducible. In this instance, the χ_{TIM} values in the solid I in the first heating run and in the solid II in the first cooling run varied, depending on the ratio of the two components. For example, **1**(80:20) [an 80:20 mixture of (*R*,*S*)-**1** and (*R**,*R**)-**1**], which was obtained by dissolving the two isolated components in CH_2Cl_2 followed by vacuum evaporation, exhibited a distinct superparamagnetic-like *M-H* behavior in the original solid I and a much larger χ_M increase at the solid I-to-Col_h phase transition in the first heating run than **1**(95:5) did (Fig. 9). According to eqs 1 and 3, $\chi_{TIM} + \chi_{dia} = +4.1 \times 10^{-4}$ emu mol^{-1}, Weiss constant $\theta = 0$ K, and Curie constant $C = 0.62$ emu K mol^{-1} were obtained in the first heating run. The χ_{TIM} values obtained by subtracting the calculated χ_{dia} value (-1.6×10^{-3} emu mol^{-1}) from the experimental ($\chi_{TIM} + \chi_{dia}$) value ($+4.1 \times 10^{-4}$, $+4.4 \times 10^{-3}$ and $+4.4 \times 10^{-3}$ emu mol^{-1}) between 100 and 250 K in the first heating and cooling runs and the second heating run were $+1.6 \times 10^{-3}$, $+6.0 \times 10^{-3}$ and $+6.0 \times 10^{-3}$ emu mol^{-1}, respectively. Absolutely, such an extraordinary χ_M or χ_{TIM} increase ($+4.4 \times 10^{-3}$ emu mol^{-1}) cannot be explained by the molecular reorientation effect due to the small molecular $\Delta\chi$.

From these experimental results, the following five facts were revealed; (1) neither pure (*R*,*S*)-**1** nor (*R**,*R**)-**1** exhibited a superparamagnetic-like behavior in the original solid phase in the first heating run, (2) pure (*R*,*S*)-**1** showed the superparamagnetic-like *M-H* behavior only by the first cooling from the isotropic phase at 0.05 T, most likely due to the partial formation of boat and/or half-chair conformers of (*R*,*S*)-**1** which are assumed to result from the thermal motion of the cyclohexane ring in the isotropic phase and serve as necessary impurities to lead to the partial formation of magnetically inhomogeneous domains, (3) the original solid I composed of major (*R*,*S*)-**1** and minor (*R**,*R**)-**1** showed the superparamagnetic-like behavior most likely because (*R**,*R**)-**1** serve as an organic impurity to form magnetically inhomogeneous domains easily, (4) such a superparamagnetic-like *M-H* behavior was not caused by either external magnetic impurities such as iron and nickel or the small molecular $\Delta\chi$, and (5) such a unique magnetic phenomenon is reminiscent of the magnetic properties of spin glass materials induced by thermal processing[40-42] or the

presence of impurity.[41,43]

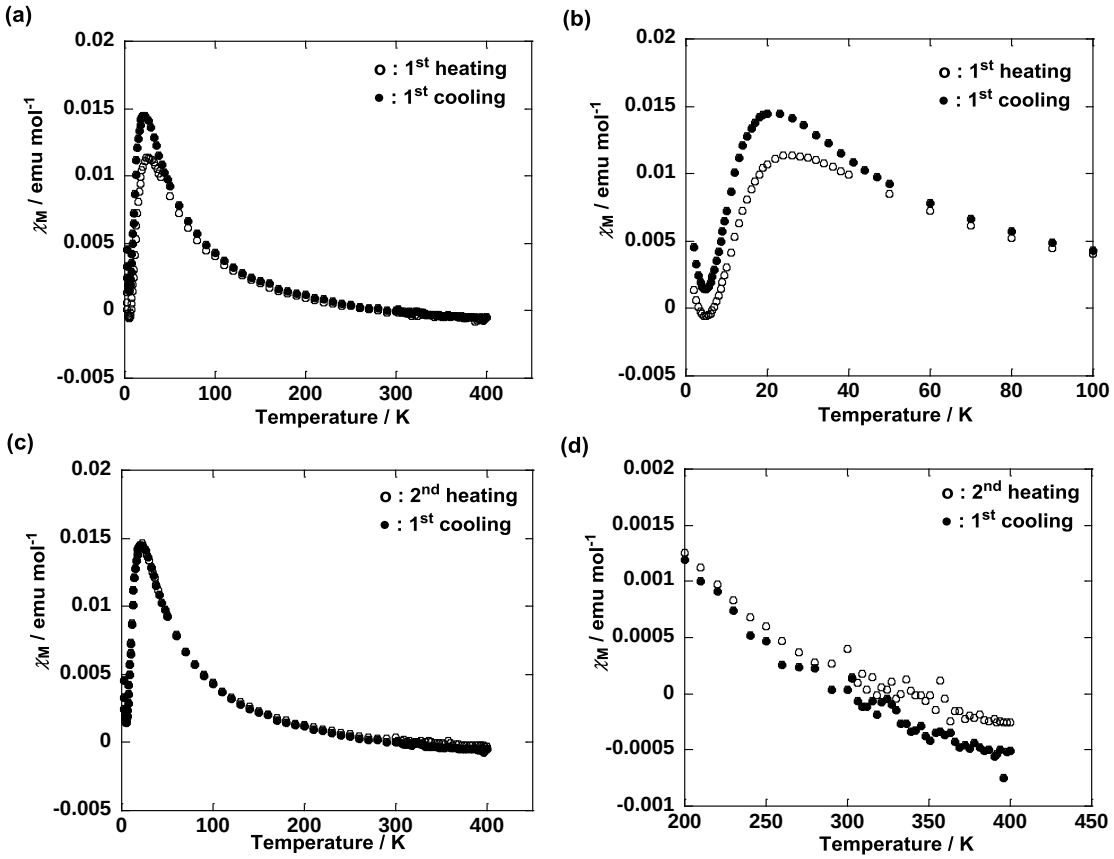

Figure 6. Temperature dependence of χ_M for (*R*,*S*)-**1** (a) in the first heating and cooling runs, (b) by magnification (between 2 and 100 K) of panel a, (c) in the first cooling and second heating runs, and (d) by magnification (between 200 and 400 K) of panel c, at 0.05 T in the temperature range between 2 and 400 K using a paramagnetic aluminum foil.

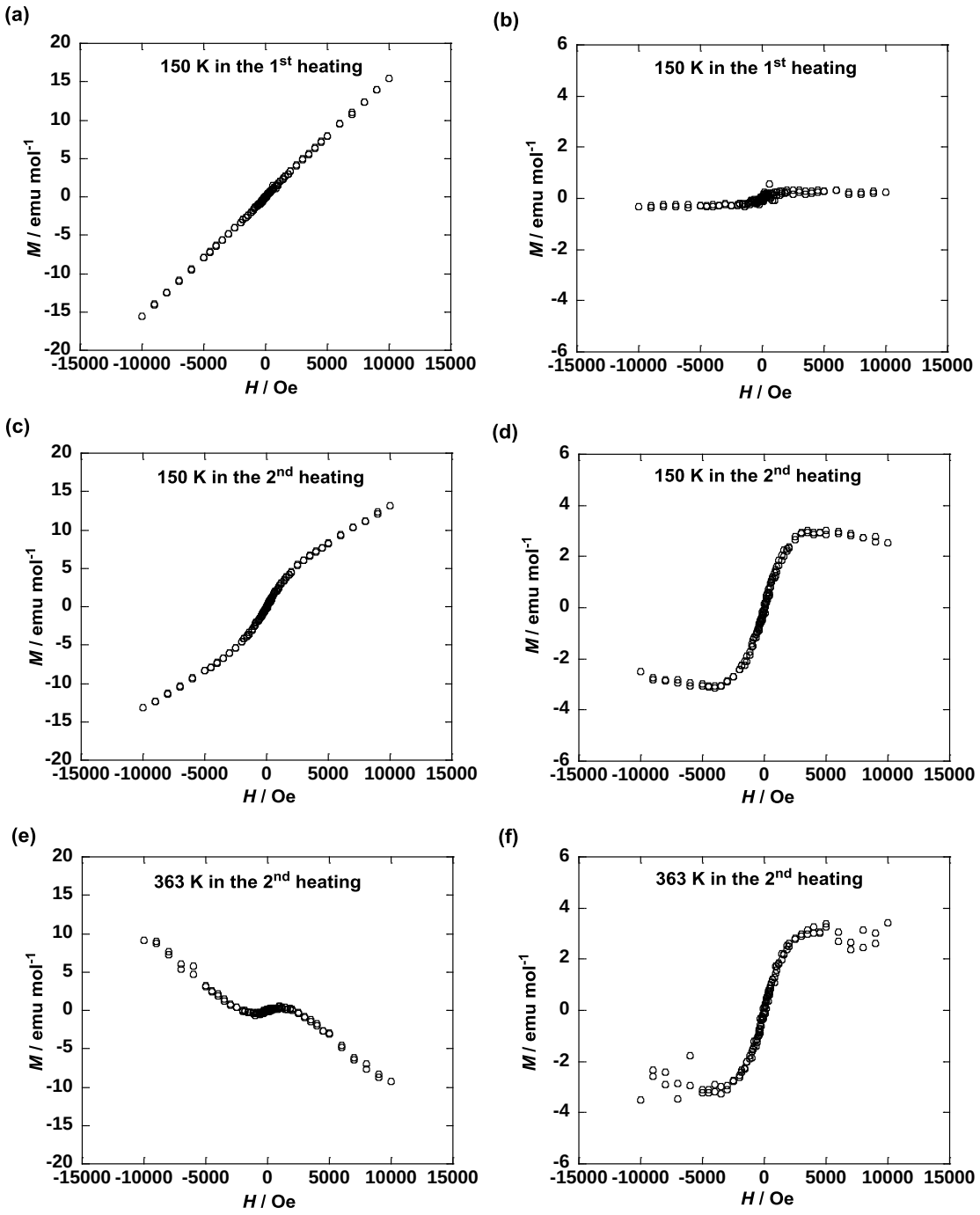

Figure 7. Magnetic field (*H*) dependence of molar magnetization (*M*) for (*R*,*S*)-**1** (a) in the solid I at 150 K by the first heating from 2 K, (b) after correction of the oblique linear base line to the horizontal one in panel a, (c) in the solid II at 150 K by the second heating after the first heating up to 400 K followed by cooling to 2 K at 0.05 T, (d) after correction of the oblique linear base line to the horizontal one in panel c, (e) in the Col_h phase at 363 K by the second heating, and (f) after correction of the oblique linear base line to the horizontal one in panel e.

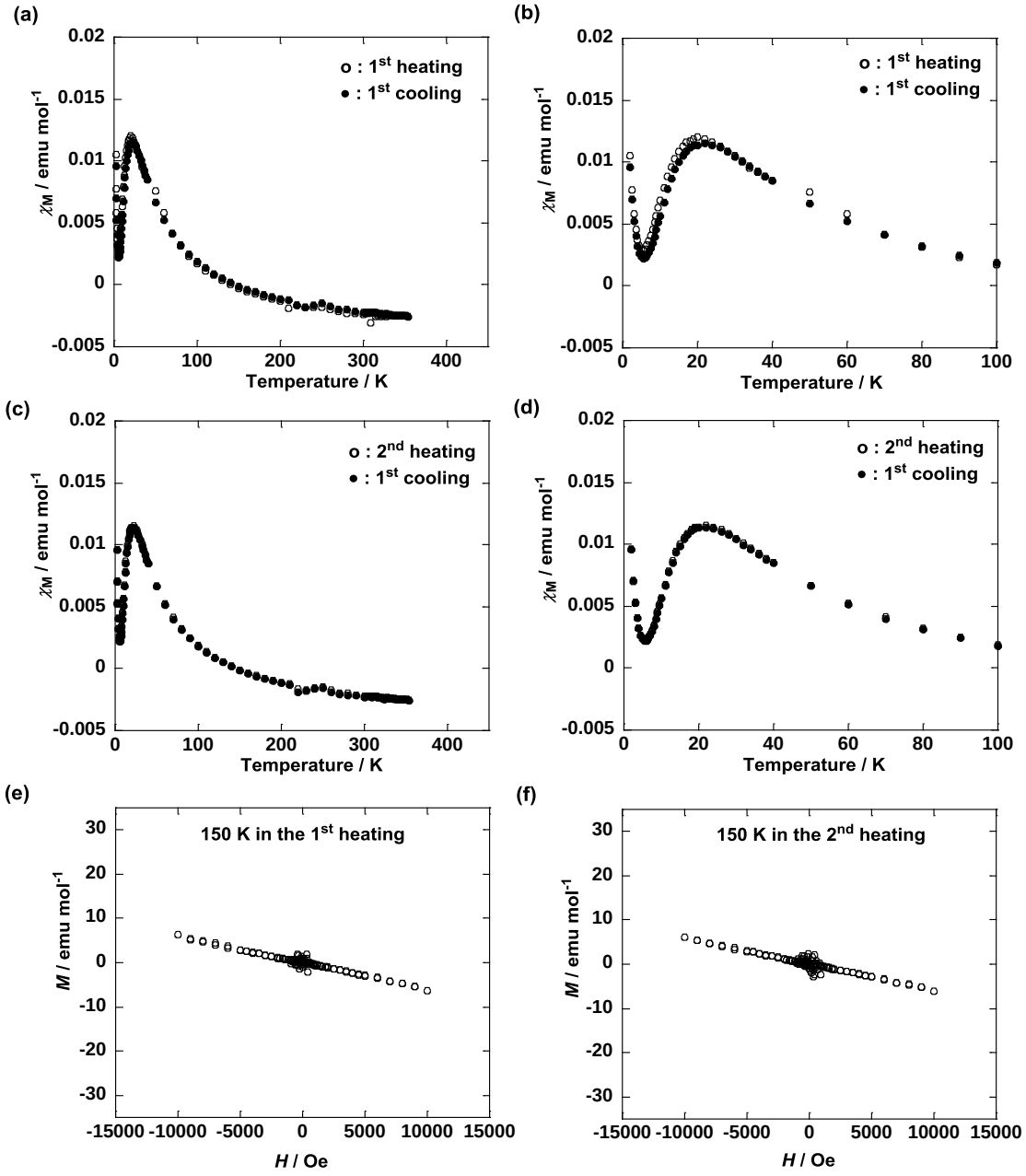

Figure 8. Temperature dependence of χ_M for (*R**,*R**)-**1** (a) in the first heating and cooling runs, (b) by magnification (between 2 and 100 K) of panel a, (c) in the first cooling and second heating runs, and (d) by magnification (between 2 and 100 K) of panel c, at 0.05 T in the temperature range between 2 and 354 K using a paramagnetic aluminum foil. Magnetic field (*H*) dependence of molar magnetization (*M*) for (*R**,*R**)-**1** in the solid phase at 150 K (e) by the first heating from 2 K and (f) by the second heating after the first heating up to 354 K followed by cooling to 2 K at 0.05 T.

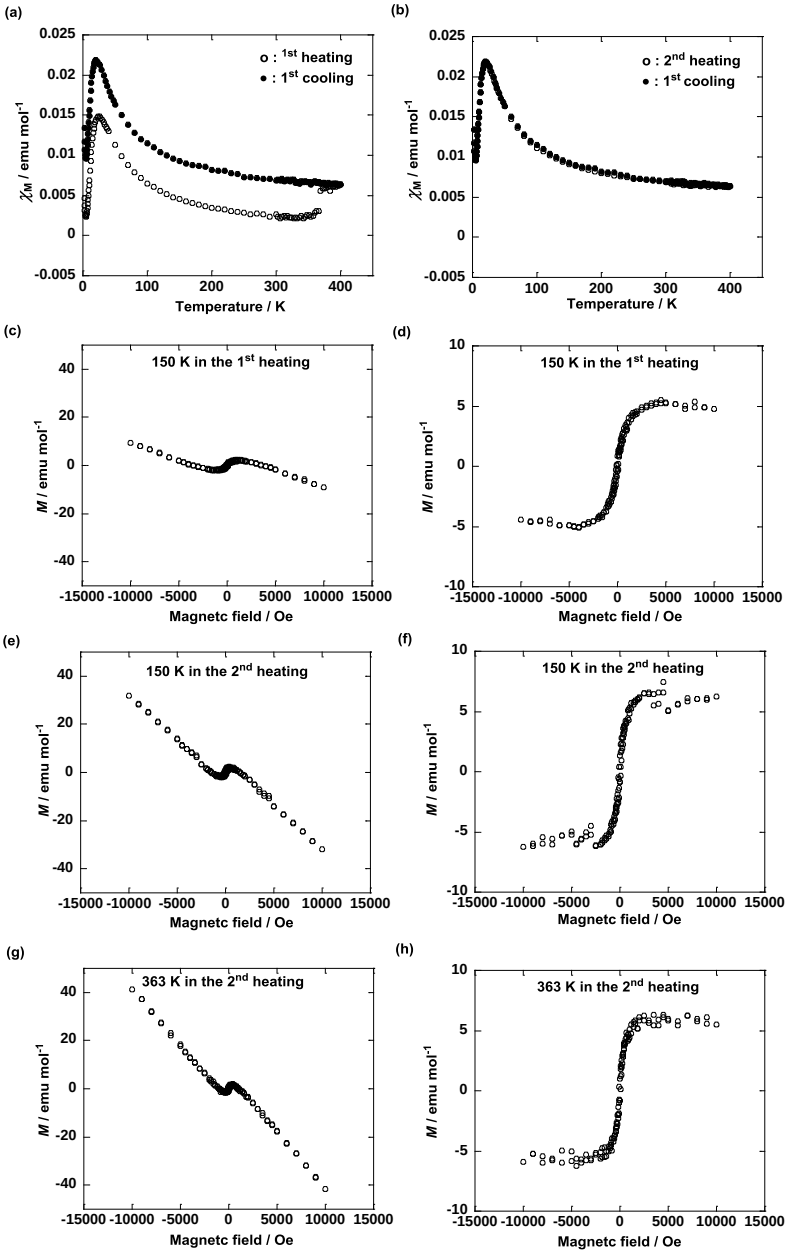

Figure 9. Temperature dependence of χ_M for **1**(80:20) (a) in the first heating and cooling runs and (b) in the first cooling and second heating runs at 0.05 T in the temperature range between 2 and 400 K using a paramagnetic aluminum foil. Magnetic field (*H*) dependence of molar magnetization (*M*) for **1**(80:20) (c) in the solid I at 150 K by the first heating from 2 K, (d) after correction of the oblique linear base line to the horizontal one in panel c, (e) in the solid II at 150 K by the second heating after the first heating up to 400 K followed by cooling to 2 K at 0.05 T, (f) after correction of the oblique linear base line to the horizontal one in panel e, (g) in the Col_h phase at 363 K by the second heating, and (h) after correction of the oblique linear base line to the horizontal one in panel g.

To gain a microscopic insight into the mechanism of the observed positive magneto-LC effect operating in the Col_h phase of **1**(95:5), the temperature dependences of EPR *g*-value and peak-to-peak line width (ΔH_{pp}) were compared with that of the χ_M (Fig. 10 a,b). The *g*-value was almost constant due to no molecular reorientation in the Col_h phase, while a large increase (more than 30%) in ΔH_{pp} occurred in accord with the increase in χ_M at the crystal-to-Col_h transition at around 80 °C in the first heating run (Fig. 4c), indicating a considerable increase in the intermolecular spin-spin dipole interactions in the Col_h phase. These results that were consistent with those observed in various rod-like LC phases of all-organic nitroxide monoradical and biradical compounds[16-19] support that strong intermolecular spin-spin dipole as well as exchange interactions should operate in the magnetically inhomogeneous domains formed in the Col_h phase to result in the χ_M and χ_{TIM} increase. The formation of magnetic interactions between the neighboring disc layers within each column by spin polarization mechanism via intermolecular CH/O interactions[44] is likely responsible for the observed magnetic phenomenon (Fig. 10c), because it was verified that both the C3 and C4 atoms on the five-membered nitroxide structure in 2,2,5-trimethyl-5-phenylpyrrolidine-1-oxy possess a positive spin density by DFT calculations (section 9 and Fig. S5 in SI).[45]

Thus far, the existence of χ_{TIM} in the original solid I and the subsequent χ_M and χ_{TIM} increases could not be correlated with the energy bands formation, which is similar to the mechanism of Pauli paramagnetism,[46] in the Col_h phase by the UV-Vis spectral and photoconductivity measurements of **1**(95:5) (Sections 10 and 11, and Figs. S6 and S7 in SI, respectively).

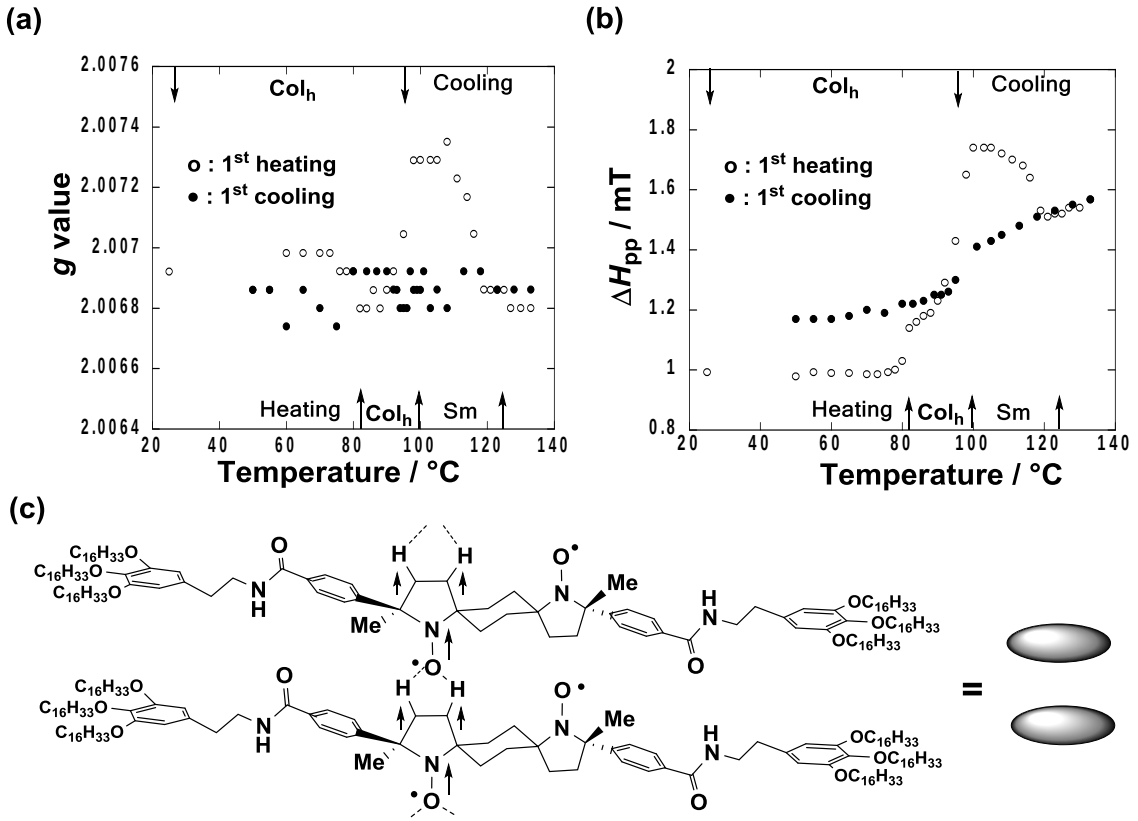

Figure 10. Temperature dependence of (a) *g*-value and (b) ΔH_{PP} for **1**(95:5) in the first heating (open circles) and cooling (closed circles) runs by EPR spectroscopy at around 0.33 T. (c) Intermolecular spin polarization via CH/O interactions between two (*R*,*S*)-**1** molecules in the neighboring disc layers expected in the magnetically inhomogeneous domains.

CONCLUSIONS

The unique magnetic properties of achiral non-π-delocalized nitroxide diradical compounds **1**, which showed a very rare coexistence of two LC phases (Col$_h$ and Sm) over a wide temperature range by very slow cooling from the isotropic phase, were investigated. The gradual formation of chiral helical columnar structure in the Col$_h$ phase was confirmed by a preliminary SHG measurement. Almost negligible contamination by extrinsic magnetic metal or metal ion impurities was proved by the ICP-AES analysis and the *H* dependence of *M* measurement for **1**(95:5), LC (*R*,*S*)-**1**, and non-LC (*R**,*R**)-**1** independently. Although pure (*R*,*S*)-**1** showed only an ordinary paramagnetic behavior in the first heating run from the original nanocrystalline solid I, the superparamagnetic-like *M*-*H* behavior was observed by the first cooling from the isotropic phase under low magnetic fields, most likely due to the partial formation of cyclohexane (boat and/or half-chair) conformers of (*R*,*S*)-**1** which are supposed to serve as the impurities to form magnetically inhomogeneous domains. Furthermore, (*R*,*S*)-**1** containing a small amount of (*R**,*R**)-**1** as an organic impurity (1) possessed a large temperature-independent magnetic susceptibility component (χ_{TIM} > 0) in the original solid I before heating, which is responsible for the observed superparamagnetic-like *M*-*H*

behavior under low magnetic fields, and (2) showed a large increase in the molar magnetic susceptibility (χ_M) (positive magneto-LC effect) at the solid I-to-Col_h transition in the first heating run at 0.05 T, which was preserved as an additional χ_{TIM} increase in the resulting nanocrystalline solid II in the cooling run. In this context, **1**(80:20) composed of a 80:20 mixture of (*R*,*S*)-**1** and (*R**,*R**)-**1** displayed an extraordinarily larger χ_M or χ_{TIM} than **1**(95:5) did. These results are consistent with the formation of magnetically inhomogeneous domains with intermolecular short contacts in the solid phase and their enlargement in the LC phase under low magnetic fields, which is reminiscent of the magnetic properties of spin glass materials induced by thermal processing or the presence of impurity.[40-43] Such an existence of a large χ_{TIM} component in the original nanocrystalline solid I of compounds **1** with a large molecular structure was not observed in the original crystalline phases of small nitroxide radical compounds showing rod-like LC phases.[16,18,19] Our theoretical studies by molecular dynamic simulations on the mechanism of a large increase in the magnetic susceptibility in the solid and LC phases will be reported in due course in terms of the influence of the coherent collective molecular motion and inhomogeneous intermolecular short contacts on the magnetic susceptibility, together with the in-depth data concerning the spin glass-like properties.

These results would provide important information for the development of metal-free magnetic advanced soft materials, such as magneto-active emulsions which are expected to be used for biomedical applications including the magnetically transportable oxidation & reduction resistant magnetic microcarrier,[47] the magnetic resonance imaging (MRI) contrast agents and the magnetic nanocarrier for a magnetically targeted drug delivery system (DDS),[48] in place of magnetoliposomes containing superparamagnetic iron oxides (magnetite Fe_3O_4 or maghemite γFe_2O_3),[49] because nitroxide radicals are known to show very low toxicity to cell and animals.[50-54+]

ASSOCIATED CONTENT

Supporting Information

The Supporting Information is available free of charge on the ACS Publications website at DOI:

Details of synthesis and characterization; X-ray structural data; DFT calculations; determination of the *Z* values; polarized micrographs; variable-temperature micro-ATR-FTIR, ICP-AES and UV-Vis spectra; measurement of photocurrent, TR-SHG and THG (PDF)

Crystallographic data for (*R*,*S*)-**2** (CIF)

AUTHOR INFORMATION

Corresponding Authors

*tamura.rui.45x@st.kyoto-u.ac.jp

ORCID

Yusa Takemoto: 0000-0002-3935-308

Elena Zaytseva: 0000-0001-6040-8639

Katsuaki Suzuki: 0000-0001-8042-9517
Naoki Yoshioka: 0000-0003-3700-9570
Yoichi Takanishi: 0000-0003-4976-0652
Masahiro Funahashi: 0000-0002-4259-0657
Yoshiaki Uchida: 0000-0001-5043-9239
Takuya Akita: 0000-0001-8998-1674
Jayeong Park: 0000-0002-6567-1142
Shuichi Sato: 0000-0003-3887-0899
Simon Clevers: 0000-0002-1377-1141
Gérard Coquerel: 0000-0001-8977-8676
Dmitrii G. Mazhukin: 0000-0002-6915-6287
Satoshi Shimono: 0000-0001-8457-6055
Masahito Sugiyama: 0000-0002-6396-7943
Hiroki Takahashi: 0000-0002-8622-8617
Jun Yamauchi: 0000-0002-9607-7226
Rui Tamura: 0000-0002-4123-6795

Author Contributions

The manuscript was written through contributions of all authors.

Notes

The authors declare no competing financial interest.

ACKNOWLEDGMENT

We thank Prof. Elena V. Boldyreva and Dr. Denis A. Rychkov, Novosibirsk State University, for the measurement of VT micro ATR-FTIR spectra. The present work was supported by JSPS KAKENHI (Grant number 26248024).

REFERENCES

(1) Goodby, J. W.; Collings, P. J.; Kato, T., Tschierske, C.; Gleeson, H. F.; Raynes. P. (eds.) *Handbook of Liquid Crystals*, 2nd edn, vol. 1-8; Wiley-VCH: Weinheim, 2014.

(2) Li, Q., Ed. *Liquid Crystals Beyond Display*; Wiley: Hoboken, 2012.

(3) Dierking, I. *Textures of Liquid Crystals*; Wiley-VCH: Weinheim, 2003.

(4) Serrano, J. –L. *Metallomesogens: Synthesis, Properties, and Applications*; Wiley-VCH: Weinheim, 1996.

(5) Dunmur, D.; Tokoroyama, K. In *Physical Properties of Organic Materials*; Demus, D.; Goodby, J.; Gray, G. W.; Spiess, H. –W.; Vill, V. Eds.; Wiley-VCH: Weinheim, 1999, pp. 102-112.

(6) Kaszynski, P. In *Magnetic Properties of Organic Materials*; Lahti, P. M. Ed.; Marcel Dekker: New

York, 1999, pp. 305-324.

(7) Griesar, K.; Hasse, W. In *Magnetic Properties of Organic Materials*; Lahti, P. M. Ed.; Marcel Dekker: New York, 1999, pp.325-344.

(8) Binnemans, K.,; Görller-Walrand, C. *Chem. Rev.* **2002**, *102*, 2303-2345.

(9) Erenstein, W.; Mathur, N. D.; Scott, J. F. *Nature* **2006**, *442*, 759-765.

(10) Rao, C. N. R.; Serrao, C. R. *J. Mater. Chem.* **2007**, *17*, 4931-4938.

(11) Felser C.; Fecher, G. H.; Balke, B. *Angew. Chem. Int. Ed.* **2007**, *46*, 668-699.

(12) Seki, S. *Magnetoelectric Response in Low-Dimensional Frustrated Spin Systems*; Springer: Tokyo, 2012.

(13) Rikken, G. L. J. A.; Raupach, E. *Nature* **1997**, *390*, 493-494.

(14) Rikken, G. L. J. A.; Raupach, E. *Nature* **2000**, *405*, 932-935.

(15) Train, C.; Gheorghe, R.; Krstic, V.; Chamoreau, L. –M.; Ovanesyan, N. S.; Rikken, G. L. J. A.; Grussele, M.; Verdaguer, M. *Nat. Mater.* **2008**, *7*, 729-734.

(16) Uchida, Y.; Suzuki, K.; Tamura, R.; Ikuma, N.; Shimono, S.; Noda, Y.; Yamauchi, J. *J. Am. Chem. Soc.* **2010**, *132*, 9746-9752.

(17) Suzuki, K.; Takemoto, Y.; Takaoka, S.; Taguchi, K.; Uchida, Y.; Mazhukin, D. G.; Grigor'ev, I. A.; Tamura, R. *Chem. Commun.* **2016**, *52*, 3935-3938.

(18) Suzuki, K.; Uchida, Y.; Tamura, R.; Shimono, S.; Yamauchi, J. *J. Mater. Chem.* **2012**, *22*, 6799-6806.

(19) Tamura, R.; Uchida, Y.; Suzuki, K. In ref. 1, vol. 8.; Wiley-VCH: Weinheim, 2014, pp. 837-864.

(20) Uchida, Y.; Tamura, R.; Ikuma, N.; Shimono, S.; Yamauchi, J.; Shimbo, Y.; Takezoe, H.; Aoki, Y.; Nohira, H. *J. Mater. Chem.* **2009**, *19*, 415-418.

(21) Suzuki, K.; Uchida, Y.; Tamura, R.; Noda, Y.; Ikuma, N.; Shimono, S.; Yamauchi, J. *Soft Matter* **2013**, *9*, 4687-4692.

(22) Suzuki, K.; Uchida, Y.; Tamura, R.; Noda, Y.; Ikuma, N.; Shimono, S.; Yamauchi, J. *Adv. Sci. Tech.* **2013**, *82*, 50-54.

(23) Tamura, R.; Uchida, Y.; Suzuki, K. In *Advances in Organic Crystal Chemistry: Comprehensive Reviews 2015*; Tamura, R.; Miyata, M. Eds.; Springer: Tokyo, 2015, pp. 689-706.

(24) Ravat, P.; Marszalek, T.; Pisula, W.; Müllen, K.; Baumgarten. M. *J. Am. Chem. Soc.* **2014**, *136*, 12860-12863.

(25) Yelamaggad, C. V.; Achalkumar, A. S.; Rao, D. S. S.; Nobusawa, M.; Akutsu, H.; Yamada, J.; Nakatsuji S. *J. Mater. Chem.* **2008**, *18*, 3433-3437.

(26) Castellanos, S.; López-Calahorra, F.; Brillas, E.; Juliá, L.; Velasco, D. *Angew. Chem. Int. Ed.* **2009**, *48*, 6515-6519.

(27) Jankowiak, A.; Pociecha, D.; Szczytko, J.; Monobe. H.; Kaszyński, P. *J. Am. Chem. Soc.* **2012**, *134*, 2465-2468.

(28) Jasiński, M.; Pociecha, D.; Monobe, H.; Szczytko, J.; Kaszyński, P. *J. Am. Chem. Soc.* **2014**, *136*,

14658-14661.

(29) Jasiński, M.; Szczytko, J.; Pociecha, D.; Monobe, H.; Kaszyński, P. *J. Am. Chem. Soc.* **2016**, *138*, 9421-9424.

(30) Suzuki, K.; Mazhukin, D. G.; Takahashi, H.; Uchida, Y.; Tamura, R.; Grigor'ev, I. G. *Heterocycles* **2009**, *78*, 3091-3099.

(31) Kunishima, M.; Kawachi, C.; Morita, J.; Terao, K.; Iwasaki, F.; Tani, S. *Tetrahedron* **1999**, *55*, 13159-13170.

(32) Michon, P.; Rassat, A. *J. Am. Chem. Soc.* **1975**, *97*, 696-700.

(33) Paquette, J. A.; Yardley, R. E.; Yu, J. W. –Y.; Eichhorn, S. H.; Maly, K. E. *New J. Chem.* **2016**, *40*, 5985-5988.

(34) Feringan, B.; Romero, P.; Serrano, J. L.; Folcia, C. L.; Etxebarria, J.; Ortega, J.; Termine, R.; Golemme, A.; Gimenez, R.; Sierra, T. *J. Am. Chem. Soc.* **2016**, *138*, 12511-12518.

(35) Setia, S.; Pal, S. K. *ChemistrySelect* **2016**, *5*, 880-885.

(36) Ban, K.; Nishizawa, K.; Ohta, K.; van de Craats, A. M.; Warman, J. M.; Yamamoto, I.; Shirai, H. *J. Mater. Chem*., **2001**, *1*, 321-331.

(37) Umadevi, S.; Radhika, S.; Sadashiva, B. K. *Liquid Crystals* **2013**, *40*, 1035-1049.

(38) Kishikawa, K.; Nakahara, S.; Nishikawa, Y.; Kohmoto, S.; Yamamoto, M. A. *J. Am. Chem. Soc.* **2005**, *127*, 2565-2571.

(39) Bleaney, B.; Bowers, K. D. *Pro. Roy. Soc. London Ser. A* **1952**, *214*, 451-465.

(40) Nagata, S.; Keesom, P. H.; Harrison, H. R. *Phys. Rev. B* **1979**, *19*, 1633-1638.

(41) Fischer, K. H.; Hertz, J. A. *Spin Glasses*; Cambridge University Press: Cambridge, 1991.

(42) Tabata, M.; Watanabe, Y.; Muto, S. *Macromol. Chem. Phys.* **2004**, 205, 1174-1178.

(43) Cannella, V.; Mydosh, J. A. *Phys. Rev. B* **1972**, *6*, 4220-4237.

(44) Vorobiev, A. Kh.; Chumakova, N. A.; Pomogailo, D. A.; Uchida, Y.; Suzuki, K.; Noda, Y.; Tamura, R. *J. Phys. Chem. B* **2014**, *118*, 1932-1942.

(45) Chumakova, N. A.; Buchachenko, A. L. *Mendeleev Commun*. **2015**, *25*, 264-266.

(46) Spaldin, N. *Magnetic Materials: Fundamentals and Device Application*; Cambridge University Press: 2003.

(47) Uchida, Y.; Iwai, Y.; Akita, T.; Mitome, T.; Suzuki, K.; Tamura, R.; Nishiyama, N. *J. Mater. Chem. B* **2014**, *2*, 4130-4133.

(48) Nagura, K.; Takemoto, Y.; Moronaga, S.; Uchida, Y.; Shimono, S.; Shiino, A.; Tanigaki, K.; Amano, T.; Yoshino, F.; Noda, Y.; Koizumi, S.; Komatsu, N.; Kato, T.; Yamauchi, J.; Tamura, R. *Chem. Eur. J.* **2017**, *23*, 15713-15720.

(49) Huang, J.; Li, Y.; Orza, A.; Lu, Q.; Guo, P.; Wang, L.; Yang, L.; Mao, H. *Adv. Funct. Mater.* **2016**, *26*, 3818-3836.

(50) Mitchell, J. B.; Xavier, S.; DeLuca, A. M.; Sowers, A. L.; Cook, J. A.,; Krishna, M. C.; Hahn, S. M.;

Russo, A. *Free Radical Biol. Med.* **2003**, *34*, 93-102.

(51) Arieli, D.; Nahmany, G.; Casap, N.; Ad-El, D.; Samuni, Y. *Free Radical Res.* **2008**, *42*, 114-123.

(52) Grigor'ev, I. A.; Tkacheva, N. I.; Morozov, S. V. *Curr. Med. Chem.* **2014**, *21*, 2839-2852.

(53) Gorodetsky, A. A.; Kirilyuk, I. A.; Khramtsov, V. V.; Komarov, D. A. *Magn. Reson. Med.* **2016**, *76*, 350-358.

(54) Kubota, H.; Komarov, D. A.; Yasui, H.; Matsumoto, S.; Inanami, O.; Kirilyuk, I. A.; Khramtsov, V. V.; Hirata, H. *Magn. Reson. Mater. Phy.* **2017**, *30*, 291-298.

For Table of Contents Only

Unique Superparamagnetic-like Behavior Observed in Non-π-delocalized Nitroxide Diradical Compounds Showing Discotic and Smectic Liquid Crystalline Phases